Desalination and Water Treatment
www.deswater.com

doi: 10.5004/dwt.2017.20525

70 (2017) 387–393
April

A study of applying green glucose-reduced graphene oxide in advanced treatment of different dyes

Ruibin Wang, Rendang Yang*, Youmao Zhang

State Key Laboratory of Pulp and Paper Engineering, Plant Micro/Nano Fiber Research Center, School of Light Industry and Engineering, South China University of Technology, Wushan Rd 381, Tianhe District, Guangzhou 510640, China, Tel. +086-87110082; Fax: +086-020-87110072; emails: rdyang@scut.edu.cn (R. Yang), wang.rb@mail.scut.edu.cn (R. Wang), 10395538@qq.com (Y. Zhang)

Received 15 September 2016; Accepted 19 January 2017

ABSTRACT

Herein, a green chemical, glucose was applied to prepare reduced graphene oxide (RGO), of which the removal performance was explored within three different dye effluents of lower concentration. The results demonstrated that the average removal capacity of RGO was as high as ~47.5 mg/g, overwhelming popular adsorbents like nanotitania, activated carbon, and graphene oxide, from initial concentration of 5 mg/L. Meanwhile, effects of adsorbent dosage and reuse cycle relating to the adsorption were also addressed. Moreover, it was found that the Langmuir isotherm and pseudo-second-order model fit the adsorption process of RGO well, with the thermodynamic analysis revealing that it was performed in a spontaneous and endothermic way. Overall, this work is targeted to establish an efficient approach applied in advanced treatment of effluents.

Keywords: Green reductive; Graphene oxide; Advanced treatment

1. Introduction

In decades, increasingly harsh law have been globally made to manage the emission of dye sewage, in which most chemicals have aromatic ring or heterocyclic ring that are highly carcinogenic and mutagenic [1–3]. Hence, to advocate advanced treatment allows of no delay. However, it is adventurist to realize this aim by setting up new devices, and may not be indiscriminately adopted. Thus, upgrading present facilities sounds more reasonable; especially, when targets to the preliminarily purified wastewater that already meets the current emission standards (still contains dyes of lower concentration). For now, many novel techniques have attracted tremendous interests, such as reverse osmosis, photocatalysis, and ions exchange. However, the generalization is still hard to facilitate owing to huge energy consumption, intricate process, and complicated production operations [4–9].

Within this context, adsorption method appears to be a decent choice, thanks to the cost-effectiveness, wide available range, and operational simplicity [10,11]. In particular, graphene derivative adsorbents have been developed as a hot topic, with recent efforts being paid on avoiding over-reduction of the raw material to be aqueous insoluble, while assuring the sustainability, thus brings a bunch of weaker reductants and methods [12–16]. Ramesha et al. [17] explored the possibility of using reduced graphene oxide (RGO) for removal of cationic or anionic dyes from aqueous solutions lower than 60 mg/L. Tiwari et al. [18] synthesized the three-dimensional RGO-based hydrogels using sodium ascorbate as reductant, this hydrogels showed excellent removal capabilities for methylene blue (~100% of 8.52 mg/L) and rhodamine B (~97% of 9.5 mg/L) due to adsorption through strong π–π stacking and anion–cation interactions. A simple one-step solvothermal strategy using sustainable precursors has been developed to prepare magnetic/RGO

* Corresponding author.

nanocomposites by Sun et al. [19], over 91% for rhodamine B and 94% for malachite green of removal efficiency were obtained, with initial concentrations varying in 0.5–4 mg/L.

In this study, we stated the fabrication of RGO using biocompatible glucose and probed its adsorption considering three different dyes of lower concentration. The results indicated that GO can be efficiently reduced to RGO as an excellent adsorbent toward different dyes. Meanwhile, effects of experimental variables (adsorbent dosage and reuse cycle) on the absorption, together with relative isotherm, kinetics, and thermodynamic were all addressed in detail. Frankly, this paper could pave the way of applying glucose-RGO in environment remediation.

2. Materials and methods

2.1. Materials

Graphite (8,000 mesh), sulfuric acid (98%), sodium nitrate, potassium permanganate, hydrogen peroxide, ammonia hydroxide (25%), glucose, nanotitania, activated carbon, methylene blue, bromocresol green, and methyl orange were all in analytic grade, and purchased from Sinopharm Chemical Reagent Co., Ltd. All solutions were prepared using deionized water.

2.2. Preparation of RGO

First, precursor graphene oxide was synthesized according to the Hummers' method [20]. Then, as-prepared GO (0.4 g) was vigorously stirred with deionized water (400 mL), in a high power ultrasonic field for 2 h. The resultant suspension was then pH adjusted using 3.2 mL of $NH_3{\cdot}H_2O$, in prior to adding 8 g of glucose with rapidly heating to 100°C and kept for 2 h. Followed filtration was utilized when applying deionized water as wash phase until pH of 7 was reached. In final, the obtained filter cake was vacuum dried at 50°C to give the powdery RGO.

2.3. Batch adsorption experiments

Batch adsorption experiments (as shown in Fig. 1) were conducted in a water bath shaker at 290 K for 40 min. The

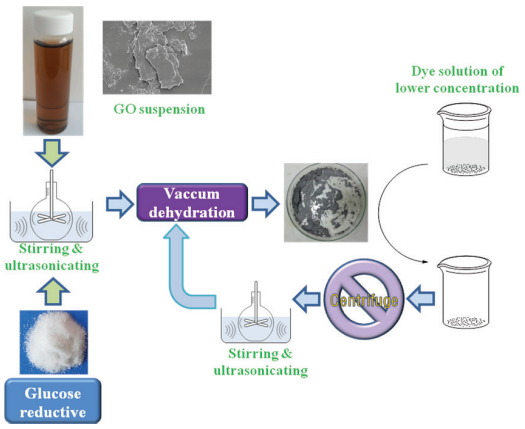

Fig. 1. Schematic experimental flow diagram showing preparation of RGO and batch adsorption experiments.

removal capacities of different adsorbents (nanotitania, activated carbon, GO, and RGO) on different dyes (methylene blue, bromocresol green, methyl orange) were tested by adding 2.5 mg of adsorbent into 20 mL dye solutions, with the concentration varying from 5 to 17.5 mg/L. After each run was done, centrifuge was conducted to separate the to-be-reused adsorbent and residual dye. In general, the adsorption capacity, a_c, and removal percentage, R%, of adsorbent (mg/g) could be evaluated with the following equations, respectively:

$$a_c = \frac{C_i - C}{m} \times V \tag{1}$$

$$R\% = \frac{C_i - C}{C_i} \times 100\% \tag{2}$$

where C_i and C are initial and final concentrations of dyes (mg/L), respectively, m is the mass of adsorbent (g), and V is volume of the solution (L).

The effect of adsorbent dosage was conducted by mixing 20 mL of dye solution (5 mg/L) with different amounts of RGO (0.05–0.15 g/L in a gradience of 0.025 g/L) at 290 K for 40 min. And the reuse cycles' study was researched by regenerating the used RGO then preceding the adsorption. In brief, the mentioned precipitate of centrifugation was concurrently stirred and ultrasonicated for 1 h as soon as re-collected, and suffered the same dehydration as described above. Thereafter, the reused RGO was obtained and could be further used in next cycle.

The adsorption isotherm was carried out by adsorbing dye solutions of different concentrations (5–17.5 mg/L, step size of 2.5 mg/L) with 2.5 mg of RGO at 290 K. Besides, the kinetics was discussed via successively investigating the adsorbing processes. Briefly, 50 mg of RGO was blended with 400 mL dye solution (10 mg/L), of which the absorbance was measured every 20 min. In addition, for the thermodynamic evaluation, 2.5 mg of RGO was mixed with 20 mL of solutions (initial concentration ranges from 5 to 17.5 mg/L, step size of 2.5 mg/L), the mixture then performed the adsorption process at different temperature (290, 307, or 324 K) for 40 min.

2.4. Characterization

Fourier transform infrared (FTIR) spectra were carried out using Bruker VERTEX 70 spectrometer in the frequency range of 3,600–400 cm^{-1} with a resolution of 4 cm^{-1}. Raman spectra were investigated on a LabRAM Aramis Raman Spectrometer in the frequency range between 500 and 3,500 cm^{-1} with a resolution of 1 cm^{-1}. X-ray photoelectron spectroscopy (XPS) was performed on a Kratos Axis Ultra DLD Spectrometer, with monochromatized Al Kα source (1,486.6 eV) under ~5 × 10^{-9} torr and scanning type of CAE. Field emission scanning electron microscope (FESEM) image was taken with a Zeiss LEO1530VP scanning electron microscope operated at 20 kV. UV–Vis spectrophotometry was conducted using an Agilent 8453 UV–visible spectrophotometer, with which the λ were fixed at 664, 463, and 615 nm with respect to methylene blue, bromocresol green, and methyl orange, respectively.

3. Results and discussion

3.1. Characterizations of RGO

The efficient transformation of GO to RGO is confirmed by the FTIR and Raman result as elucidated in Fig. 2. It is obvious that peaks around 1,101, 1,621, 1,732, and 3,138 cm^{-1} can be assigned to functional groups like C–O, C–O–C, C=O, and O–H, respectively, are shown in the spectra of GO. For RGO, almost all bands suffer a marked intensity decrease, for instance, C=C and C=O stretching vibrations can hardly be observed. Nevertheless, the weirdly steady band at 3,412 cm^{-1} gives a hint that certain fraction of hydroxyl functionality remains after the reduction (Fig. 2(a)). The Raman spectra of GO and RGO in Fig. 2(b) share two same sharp peaks, ~1,331 cm^{-1} (peak D) that is barely seen in pristine graphite and ~1,580 cm^{-1} (peak G). Thus, confirms that to some extent, RGO resembles GO, though, which is reduced by glucose, but through less severe process. Besides, the intensity ratio (I_D/I_G, peak D over peak G) of GO is about 0.9980, lower than 1.3226 of RGO. Hence, less oxygen-contained defects are included in RGO [21].

XPS is used to investigate the chemical structure and composition of all samples. As illustrated in Fig. 2, the C1s band of GO is well within agreement with databases, while RGO is significantly different. On one hand, the C/O atomic ratio of RGO significantly increases to 8.81, from 1.82 of GO (Fig. 3(a)). The decreased content of O atoms suggests that GO is successfully reduced. On the other hand, the observed XPS peaks are identified as C atoms that associate with non-covalent C–O interaction (283.0 eV), unoxidized or aromatic sp^2 structure (284.5 eV), C–C component (285.5 eV), and hydroxyl or epoxy groups (286.6 eV). It is noteworthy that GO have notable peaks around 283.0 and 285.0 eV, which are all absent in the profile of RGO. This could be presumed that after the reduction, the decreased oxygen-containing functional groups mainly affects the non-covalent bonding, meanwhile, the originally merged 285.0 eV peak split back into bands around 284.5 and 285.5 eV. As a result, glucose can be ascertained mild and sufficient for GO, as previously discussed [22].

3.2. Adsorption of dyes

3.2.1. Batch adsorption experiments

Results of different adsorbents adsorbing multiple dyes of lower concentrations are graphed in Fig. 4. Note that, in comparison to raw GO, RGO can remove ~40% more of each dye, in value. RGO shows no selectivity, otherwise insensitivity will be seen toward one (activated carbon) or two dyes (nanotitania). These may be possibly due to that RGO possesses

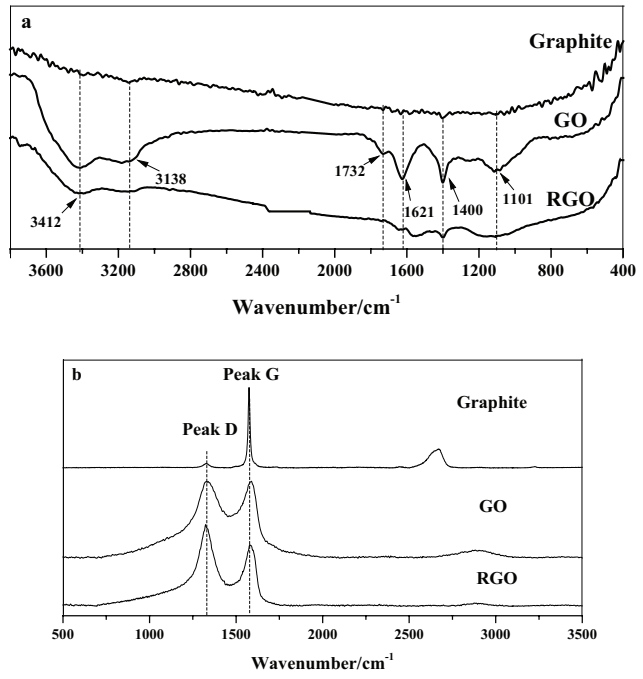

Fig. 2. (a) FTIR spectra of graphite, GO, and RGO in the range of 3,800–400 cm^{-1} and (b) Raman spectra of graphite, GO, and RGO in the range of 500–3,500 cm^{-1}.

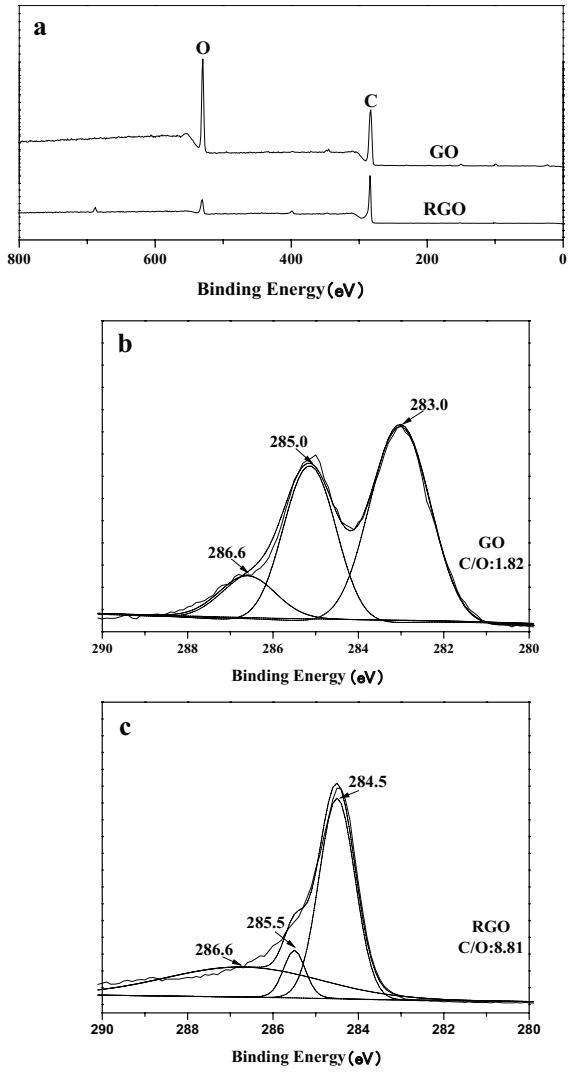

Fig. 3. (a) XPS spectra of GO and RGO in the range of 800–0 eV, (b) C1s of GO, and (c) C1s of RGO.

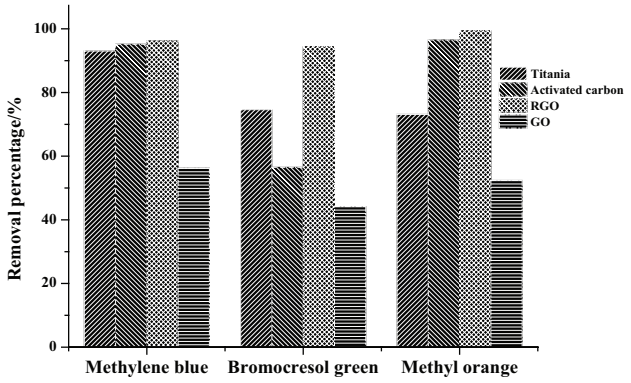

Fig. 4. Batch adsorption experiments of methylene blue, bromocresol green, and methyl orange adsorbed by nanotitania, activated carbon, and RGO, respectively.

less structural defects, namely higher non-polarity, which resulting in better affinity toward organic dye in molecules. Furthermore, since both nanotitania and activated carbon are inorganic materials, it is undoubted that the two-dimensional structure of RGO, and probable π–π interactions between RGO and aromatic rings of dyes also make difference.

3.2.2. Effects of adsorbent dosage and reuse cycle

The effect of adsorbent dosage on adsorption of methylene blue is shown in Fig. 5(a). As the adsorbent dosage increases from 0.05 to 0.15 g/L, the *R*% relatively grows from 43.1% to 96.8%, whereas the a_c reduces from 64.6 to 48.4 mg/g. Sure, higher dosage leads to increased *R*% [23]. However, the adsorption capacity is different. As a_c presents an enhancement at first, and then decreases even increasing the dosage. This may be due to that once saturation is reached, continue adding more adsorbent will cause an excess, instead of an improved adsorption capacity [24]. In general, both lacking and overdose would result in inefficiency (lower *R*% or higher cost). Therefore, the optimum adsorbent dosage of 0.1 g/L was selected for further studies.

Fig. 5(b) shows the relation between the reuse cycle and the adsorption of methylene blue. The *R*% deceases from 96.19% to 91. 91% as the reuse cycle rises to 5. This indicates that good adsorption efficiency of RGO can be recovered by the regeneration process, thanks to the surface morphology of RGO as shown in Fig. 5(c). The surface of RGO sheet grows countless folds and trenches, which benefits dye molecules to anchor and even interact, through hydrogen bonding, electrostatic interactions, and conjugated π electrons in sp^2 carbon populations [25–27]. Similarly, facile retention makes the loaded dye molecules more reachable, and can be desorbed by drastic agitation and ultrasonication of the regeneration. In addition, the slight downtrend of *R*% may be owing to some tiny cavities on RGO that are susceptible to be blocked, while which the morphology of RGO is relatively steady through the generation process [28].

3.2.3. Adsorption isotherm

To describe the interactive behavior between adsorbent and adsorbate, it is adsorption isotherm the most important

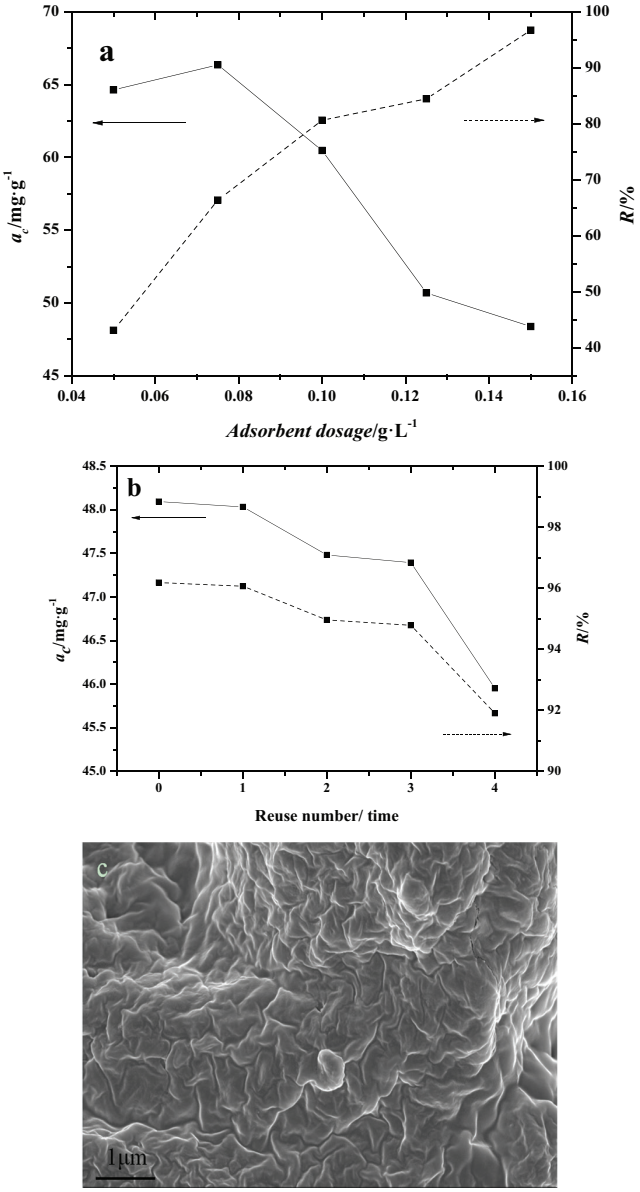

Fig. 5. (a) Effect of adsorbent dosage on methylene blue adsorbed by RGO, (b) effect of reuse numbers on the adsorption of methylene blue, and (c) high magnification FESEM image of RGO.

design parameter. Based on this, methylene blue is specified as the research object due to RGO possesses unobvious selectivity against different types of dyes. Fig. 6 shows the adsorption isotherm of methylene blue absorbed by RGO. When the *C* is lower, the adsorption capacity increases sharply, which indicates that plenty of active sites are accessible. However, if increases the *C*, the escalating trend of a_c will slow down or even stop changing. This may be attributed to that though continue increasing *C*, overmuch dye can hardly diffuse into saturated pores or crevices of the adsorbent, once the equilibrium was already reached.

The adsorption isotherm data are commonly visualized to models, namely the Langmuir equation [29], BET equation [30], Kelvin equation [31], and Dubinin

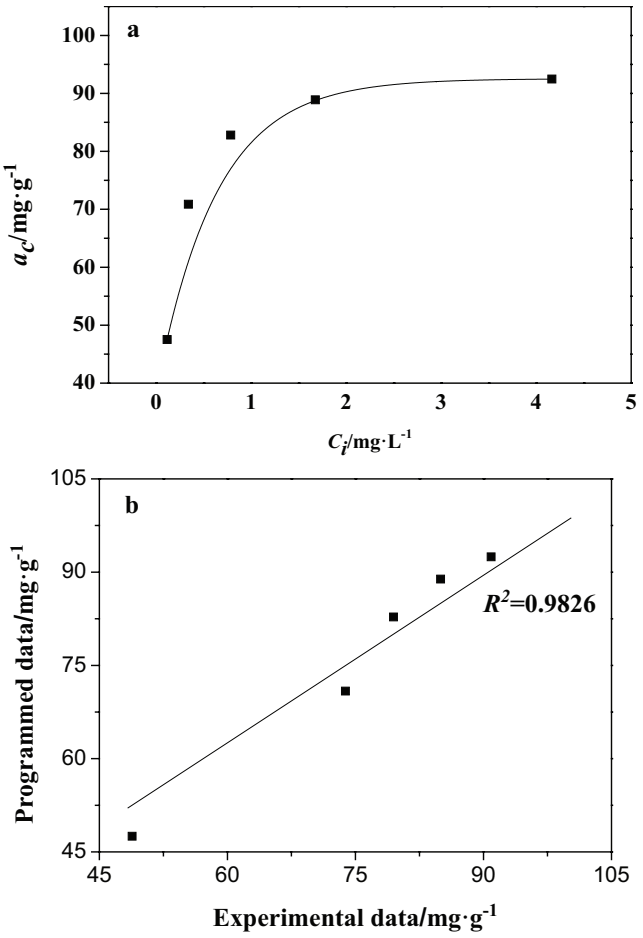

Fig. 6. (a) The Langmuir isotherm of methylene blue adsorbed by RGO and (b) outcome assessment of fitting the experimental data according to the Langmuir isotherm theory.

equation [32]. The Langmuir equation hypothesizes that the adsorption process happens on a homogeneous surface in the monolayer pattern, and the sorption energies are equivalent. The Langmuir equation can be expressed as:

$$a_c = \frac{L_c a_{\max} C}{1 + L_c C} \tag{3}$$

where C (mg/L) is the final concentration of methylene blue, $a_{\max}$ (mg/g) represents the maximum adsorption capacity, L_c (L/mg) is the Langmuir constant related to the energy of adsorption and represents the affinity within adsorbent and adsorbate. The values of $a_{\max}$ and L_c were programmed by using Eq. (3) to fit the adsorption isotherm data and they are 93.49 mg/g and 5.16 L/mg, respectively. It is 0.9826 the determination coefficient of the Langmuir equation, which suggests that the Langmuir equation can be used in this experiment to assess the maximum dye adsorption capacity. The Langmuir isotherm can be expressed as a dimensionless parameter (L_i):

$$L_i = \frac{1}{1 + L_c C_i} \tag{4}$$

where C_i is the highest initial concentration of methylene blue (mg/L), the value of L_i indicates that whether the discussed Langmuir isotherm is favorable ($0 < L_i < 1$) or not ($L_i > 1$ means unfavorable, $L_i = 1$ means linear, $L_i = 0$ means irreversible). In this study, the calculated L_i is 0.01, indicating that methylene blue adsorbed by RGO is favorable [33–36].

3.2.4. Kinetic studies

In order to evaluate the kinetic mechanism that manages the whole adsorption process, the pseudo-first-order equation and the pseudo-second-order equation were applied to analyze the experimental data. The pseudo-first-order equation was expressed as follows:

$$\ln\left(a_e - a_t\right) = \ln\left(a_e\right) - \frac{k_1}{2.303} t \tag{5}$$

where k_1 is the rate constant of pseudo-first-order adsorption (1/min), a_e and a_t are the amounts of methylene blue adsorbed at equilibrium and at time t (min), respectively. The values of k_1 and a_e can be calculated from the slope of the plots of $\ln(a_e - a_t)$ vs. t (Fig. 7(a)) and they are 0.042/min and 163.5 mg/g, respectively. The determination coefficient r^2 is as lower as 0.4018, which indicates the data disobey the pseudo-first-order kinetic model.

The linearized-integral form of the pseudo-second-order model is expressed as follows:

$$\frac{t}{a_t} = \frac{1}{k_2 a_e^2} + \frac{t}{a_e} \tag{6}$$

where k_2 (g/(mg·min)) is the rate constant of pseudo-second-order adsorption. From the slope and vertical intercept of the linear charts obtained by plotting t/a_t against t (Fig. 7(b)), k_2 and a_e can be calculated and the values are given as 0.364 mg/(mg·min) and 95.2 mg/g, respectively. However, higher determination coefficient (0.9933) and closer experimental data (90.4 mg/g) imply that the adsorption of methylene blue onto RGO fits the pseudo-second-order model well. Moreover, the overall rate of the dye adsorption is likely monitored by chemically sharing of electrons or by covalently exchanging of electrons between adsorbent and adsorbate [37].

3.2.5. Thermodynamic studies

Aiming to appraise the contribution of temperature in this experiment, the thermodynamic parameters, for instance, Gibbs free energy (ΔG), standard enthalpy change (ΔH), and standard entropy change (ΔS) are calculated at different temperature using the following equations:

$$\Delta G = -RT \ln\left(L_c\right) \tag{7}$$

$$\Delta G = \Delta H - T\Delta S \tag{8}$$

$$\ln\left(L_c\right)=\frac{\Delta S}{R}-\frac{\Delta H}{RT} \tag{9}$$

where R (8.3145 J/(mol·K)) is the universal gas constant, L_c (L/g) is the Langmuir constant, and T (K) is the absolute temperature (in Kelvin). The values of ΔH and ΔS can be calculated from the slopes and the intercept of the linear straight by plotting $\ln(L_c)$ against $1/T$, and the values of ΔG can be calculated in accordance to Eq. (9). Table 1 shows the values of ΔH, ΔS and ΔG at different initial dye concentrations and temperatures.

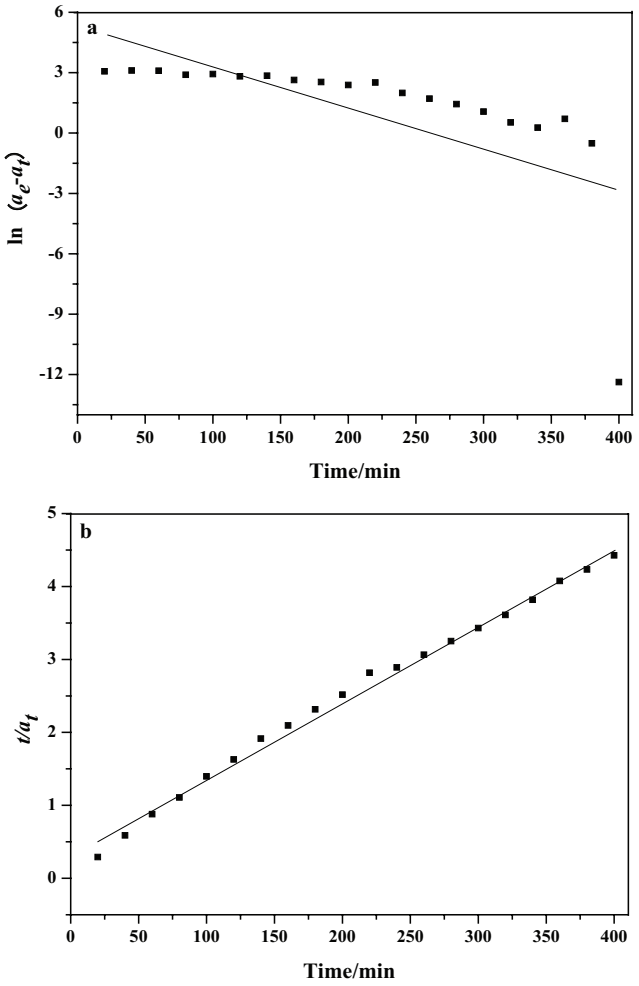

Fig. 7. Fitting of methylene blue adsorbed by RGO with (a) the pseudo-first-order equation and (b) the pseudo-second-order equation.

Table 1
Thermodynamic parameters for RGO adsorbing methylene blue

T (K)	L_c (L/g)	ΔH (kJ/mol)	ΔS (J/mol·K)	ΔG (kJ/mol)
290	5.16	19.28	80.30	–4.01
307	8.59			–5.37
324	11.91			–6.74

The negative value of ΔG indicates that the adsorption of methylene blue dye onto RGO is a spontaneous and feasible process. And the absolute value of ΔG between 0 and 20 proves this adsorption process is a physisorption; in particular, it increases as the temperature grows, and suggests the adsorption is more favorable at higher temperature. The positive standard enthalpy change (ΔH) suggests that the adsorption is an endothermic reaction, and the positive standard entropy change (ΔS) reveals the increased randomness at the solid–solution interface during the adsorption progress [38]. As temperature increases, the enhanced mobility of dye molecules causes themselves to escape from the solid phase to the liquid phase, and the amount of methylene blue adsorbed by RGO consequently increases [36,39].

4. Conclusions

Since environment laws and legislations are growing stricter, nowadays, acceptable sewage that contains dye of lower concentration will need the advanced treatment before long. Therefore, the initial target here is to engineer a suitable removal agent. In this study, the sustainable glucose not only efficiently RGO (the I_D/I_G and C/O ratio increased to 1.3226 and 8.8, respectively), but also gave RGO an average removal capacity of ~47.5 mg/g, unselectively against methylene blue, bromocresol green, and methyl orange. Furthermore, RGO is verified to have good recyclability that an R% of over 91% is displayed even after five reuse cycles. In addition, the adsorption of RGO can be best described by the Langmuir isotherm (R^2 of 0.9826) and the pseudo-second-order kinetic model (R^2 of 0.9933). While the thermodynamic study proved it by concerning a spontaneous and endothermic course in the case of physisorption. Overall, the green glucose-RGO is expected to improve the water security in the near future.

Acknowledgment

The authors wish to thank the 111 plan and Guangdong provincial science and technology plan projects of 2015B020241001 for financial support of this study.

References

[1] S. Kuppusamy, P. Thavamani, M. Megharaj, K. Venkateswarlu, Y. Lee, R. Naidu, Oak (*Quercus robur*) acorn peel as a low-cost adsorbent for hexavalent chromium removal from aquatic ecosystems and industrial effluents, Water Air Soil Pollut., 227 (2016) 1–11.
[2] H.J. Hou, R.H. Zhou, P. Wu, L. Wu, Removal of Congo red dye from aqueous solution with hydroxyapatite/chitosan composite, Chem. Eng. J., 211–212 (2012) 336–342.
[3] L.I. Doumic, P.A. Soares, M.A. Ayude, M. Cassanello, R. Boaventura, V.P. Vilar, Enhancement of a solar photo-Fenton reaction by using ferrioxalate complexes for the treatment of a synthetic cotton-textile dyeing wastewater, Chem. Eng. J., 277 (2015) 86–96.
[4] S. Pradhan, L. Fan, F.A. Roddick, Removing organic and nitrogen content from a highly saline municipal wastewater reverse osmosis concentrate by UV/H_2O_2-BAC treatment, Chemosphere, 136 (2015) 198–203.
[5] N. Uzal, L. Yilmaz, U. Yetis, Nanofiltration and reverse osmosis for reuse of indigo dye rinsing waters, Sep. Sci. Technol., 45 (2010) 331–338.
[6] R. Wang, R. Yang, B. Wang, W. Gao, Efficient degradation of methylene blue by the nano TiO_2-functionalized graphene

oxide nanocomposite photocatalyst for wastewater treatment, Water Air Soil Pollut., 227 (2016) 1–9.
[7] S. Lim, T. Kim, Removal of organic matter and nitrogen in swine wastewater using an integrated ion exchange and bioelectrochemical system, Bioresour. Technol., 189 (2015) 107–112.
[8] X. Cai, B. Zhang, L. Shi, H. Liu, J. Zhang, L. Huang, S. Tan, Study the photocatalysis activity of hydrothermal-synthesized $BiVO_4$-graphene composite on methylene blue, Desal. Wat. Treat., 57 (2016) 6365–6371.
[9] S. Maleki, M. Mirzaei, A. Azimi, COD reduction by TiO_2/graphene photocatalytic treatment of ethylene dichloride in wastewater, Desal. Wat. Treat., 57 (2016) 13207–13212.
[10] X. Liu, H. Hong, X. Wu, Y. Wu, Y. Ma, W. Guan, Y. Ye, Synthesis of TiO_2-reduced graphene oxide nanocomposites for efficient adsorption and photodegradation of herbicides, Water Air Soil Pollut., 227 (2016) 1–8.
[11] S. Chatterjee, D. Lee, M. Lee, S. Woo, Enhanced adsorption of congo red from aqueous solutions by chitosan hydrogel beads impregnated with cetyl trimethyl ammonium bromide, Bioresour. Technol., 100 (2009) 2803–2809.
[12] M. Fernandez-Merino, L. Guardia, J. Paredes, S. Villar-Rodil, P. Solis-Fernandez, A. Martinez-Alonso, J. Tascon, Vitamin C is an ideal substitute for hydrazine in the reduction of graphene oxide suspensions, J. Phys. Chem., 114 (2010) 6426–6432.
[13] O. Moradi, M. Yari, K. Zare, B. Mirza, F. Najafi, Carbon nanotubes: a review of chemistry principles and reactions, Fullerenes Nanotubes Carbon Nanostruct., 20 (2012) 138–151.
[14] A. Ahmadpour, N. Eftekhari, A. Ayati, Performance of MWCNTs and a low-cost adsorbent for Chromium (VI) ion removal, J. Nanostruct. Chem., 4 (2014) 171–178.
[15] K. Zare, V. Gupta, O. Moradi, A. Makhlou, M. Sillanpää, M. Nadagouda, H. Sadegh, R. Shahryari-ghoshekandi, A. Pal, Z. Wang, I. Tyagi, M. Kazemi, A comparative study on the basis of adsorption capacity between CNTs and activated carbon as adsorbents for removal of noxious synthetic dyes: a review, J. Nanostruct. Chem., 5 (2015) 227–236.
[16] S. Sahebian, S. Zebarjad, J. Khaki, A. Lazzeri, A study on the dependence of structure of multi-walled carbon nanotubes on acid treatment, J. Nanostruct. Chem., 5 (2015) 287–293.
[17] G. Ramesha, A. Kumara, H. Muralidhara, S. Sampath, Graphene and graphene oxide as effective adsorbents toward anionic and cationic dyes, J. Colloid Interface Sci., 361 (2011) 270–277.
[18] J. Tiwari, K. Mahesh, N. Le, K. Kemp, R. Timilsina, R. Tiwari, K. Kim, Reduced graphene oxide-based hydrogels for the efficient capture of dye pollutants from aqueous solutions, Carbon, 56 (2013) 173–182.
[19] H. Sun, L. Cao, L. Lu, Magnetite/reduced graphene oxide nanocomposites: one step solvothermal synthesis and use as a novel platform for removal of dye pollutants, Nano Res., 4 (2010) 550–562.
[20] W. Hummers Jr., R. Offeman, Preparation of graphitic oxide, J. Am. Chem. Soc., 80 (1958) 1339.
[21] F. Tuinstra, J. Koenig, Raman spectrum of graphite, J. Chem. Phys., 53 (1970) 1126–1130.
[22] H. Feng, R. Cheng, X. Zhao, X. Duan, J. Li, A low-temperature method to produce highly reduced graphene oxide, Nat. Commun., 4 (2013) 1539–1546.
[23] B. Hameed, Evaluation of papaya seeds as a novel non-conventional low-cost adsorbent for removal of methylene blue, J. Hazard. Mater., 162 (2009) 939–944.
[24] Y. Li, Z. Luan, X. Xiao, X. Zhou, C. Xu, D. Wu, B. Wei, Removal of Cu^{2+} ions from aqueous solutions by carbon nanotubes, Adsorpt. Sci. Technol., 21 (2003) 475–485.
[25] S. Pei, H. Cheng, The reduction of graphene oxide, Carbon, 50 (2012) 3210–3228.
[26] D. Dreyer, S. Park, C. Bielawski, R. Ruoff, The chemistry of graphene oxide, Chem. Soc. Rev., 39 (2010) 228–240.
[27] K. Loh, Q. Bao, P. Ang, J. Yang, The chemistry of grapheme, J. Mater. Chem., 20 (2010) 2277–2289.
[28] Q. Du, J. Sun, Y. Li, X. Yang, X. Wang, Z. Wang, L. Xia, Highly enhanced adsorption of congo red onto graphene oxide/chitosan fibers by wet-chemical etching off silica nanoparticles, Chem. Eng. J., 245 (2014) 99–106.
[29] I. Langmuir, The adsorption of gases on plane surfaces of glass, mica and platinum, J. Am. Chem. Soc., 40 (1918) 1361–1403.
[30] S. Brunauer, P. Emmett, E. Teller, Adsorption of gases in multimolecular layers, J. Am. Chem. Soc., 60 (1938) 309–319.
[31] W. Thomson, 4. On the equilibrium of vapour at a curved surface of liquid, Proc. R. Soc. Edinburgh, 7 (1872) 63–68.
[32] M. Dubinin, L. Radushkevich, Equation of the characteristic curve of activated charcoal, Chem. Zentralbl., 1 (1947) 875–890.
[33] M. Chen, Y. Chen, G.W. Diao, Adsorption kinetics and thermodynamic of methylene blue onto *p-tert*-butyl-calix[4,6,8] arene-bonded silica gel, J. Chem. Eng. Data, 55 (2010) 5109–5116.
[34] O. Moradi, M. Aghaie, K. Zare, M. Monajjemi, H. Aghaie, The study of adsorption characteristics Cu^{2+} and Pb^{2+} ions onto PHEMA and P(MMA-HEMA) surfaces from aqueous single solution, J. Hazard. Mater., 170 (2009) 673–679.
[35] O. Moradi, K. Zare, M. Monajjemi, M. Yari, H. Aghaie, The studies of equilibrium and thermodynamic adsorption of Pb(II), Cd(II) and Cu(II) ions from aqueous solution onto SWCNTs and SWCNT–COOH surfaces, Fullerenes Nanotubes Carbon Nanostruct., 18 (2010) 285–302.
[36] P. Serife, E. Volkan, A. Ahmet, P. Erol, Removal of chromium (VI) using activated carbon-supported-functionalized carbon nanotubes, J. Nanostruct. Chem., 5 (2015) 255–263.
[37] D. Malik, V. Strelk Jr., M. Strat, A. Puziy, Characterisation of novel modified active carbons and marine algal biomass for the selective adsorption of lead, Water Res., 36 (2002) 1527–1538.
[38] F. Zare, M. Ghaedi, A. Daneshfar, S. Agarwal, I. Tyagi, T. Saleh, V. Gupta, Efficient removal of radioactive uranium from solvent phase using AgOH-MWCNTs nanoparticles: kinetic and thermodynamic study, Chem. Eng. J., 273 (2015) 296–306.
[39] A. Petranovska, N. Abramov, S. Turanska, P. Gorbyk, A. Kaminskiy, N. Kusyak, Adsorption of *cis*-dichlorodiammineplatinum by nanostructures based on single-domain magnetite, J. Nanostruct. Chem., 5 (2015) 275–285.